

Commissioning of the highly granular SiW-ECAL technological prototype

S. Bilokin¹, J. Bonis, P. Cornebise, A. Gallas, A. Irles^{}, R. Pöschl, F. Richard, A. Thiebault, D. Zerwas**

Laboratoire de l'Accélérateur Linéaire, CNRS/IN2P3 et Université de Paris-Sud XI, Centre Scientifique d'Orsay Bâtiment 200, BP 34, F-91898 Orsay CEDEX, France

M. Anduze, V. Balagura, V. Boudry, J.-C. Brient, E. Edy, G. Fayolle, M. Frotin, F. Gastaldi, A. Lobanov, F. Magniette, J. Nanni, M. Rubio-Roy², K. Shpak, H. Videau, D. Yu³
Laboratoire Leprince-Ringuet (LLR) – École Polytechnique, CNRS/IN2P3, Palaiseau, F-91128 France

S. Callier, F. Dulucq, Ch. de la Taille, N. Seguin-Moreau

Laboratoire OMEGA – École Polytechnique-CNRS/IN2P3, Palaiseau, F-91128 France

J.E. Augustin, R. Cornat, J. David, P. Ghislain, D. Lacour, L. Lavergne⁴, J.M. Parraud
Laboratoire de Physique Nucléaire et de Hautes Energies (LPNHE), Sorbonne Université, UPD, CNRS/IN2P3, 4 Place Jussieu, 75005 Paris, France

K. Kawagoe, Y. Miura, I. Sekiya, T. Suehara, T. Yoshioka,

Department of Physics and Research Center for Advanced Particle Physics, Kyushu University, 744 Motoooka, Nishi-ku, Fukuoka 819-0395, Japan

D. Jeans

Institute of Particle and Nuclear Studies, KEK, 1-1 Oho, Tsukuba, Ibaraki 305-0801, Japan

J. S. Chai

Department of Electrical and Computer Engineering, Sungkyunkwan University, 16419, Suwon, Gyeonggi-do, Korea

**** Corresponding author: A. Irles, irles@lal.in2p3.fr**

ABSTRACT: In this article we describe the commissioning and a first analysis of the the beam test performance of a small prototype of a highly granular silicon tungsten calorimeter. The prototype features detector elements with a channel number similar to that envisaged for e.g. the ILD Detector of the International Linear Collider (ILC). The analysis demonstrates the capability of the detector to record signals as low as 0.5 MIP. Further, no loss of performance has been observed when operating the detector in a high magnetic field.

KEYWORDS: Calorimeter methods, calorimeters, Si and pad detectors

¹ Now at IPHC, Strasbourg.

² Now at Spintec, Grenoble

³ Now at IHEP, Beijing.

⁴ Now at IRAP, Toulouse.

Contents

1	Introduction	1
2	The SiW-ECAL technological prototype	2
2.1	Silicon sensors	2
2.2	SKIROC: Silicon pin Kalorimeter Integrated ReadOut Chip	3
2.3	Active Sensor Units	3
2.4	Data AcQuisition system	5
2.5	The prototype setup	5
3	Commissioning	7
3.1	Tagging and control of the noisy channels.	8
3.2	Optimal trigger threshold determination	9
3.3	S/N ratio for the trigger decision	10
3.4	Prospects	11
4	Performance in a beam test with positrons at DESY	12
4.1	Noise study and MIP calibration	13
4.1.1	S/N for the charge measurement of triggered channels	16
4.2	Pedestal and noise stability in a magnetic field	16
4.3	Pedestal stability in electromagnetic shower events	16
5	Summary	17
6	Outlook	18
A	Appendix: Filtering of fake triggers	19

1 Introduction

Future accelerator based particle physics experiments require very precise and detailed reconstruction of the final states produced in the beam collisions. A particular example is the next generation of e^+e^- linear colliders such the ILC[1–5]. This project will provide collisions of polarized beams with center-of-mass energies of 250 GeV to 1 TeV studied by multipurpose detectors. Two projects are proposed: the International Large Detector (ILD) and the Silicon Detector (SiD)[5]. To meet the precision required by the ILC physics goals, event reconstruction is based on the Particle Flow (PF) technique [6–8]. PF implies the reconstruction of every single particle of the final state. This in turn requires the construction of calorimeters with unprecedented granularity.

The CALICE collaboration is driving most of the efforts on R&D of highly granular calorimeters for future linear colliders by investigating and building prototypes for several calorimeter concepts. One of these calorimeters is the silicon-tungsten electromagnetic calorimeter, SiW-ECAL. Sensors made of pixellated Silicon diodes (Si) are sandwiched between tungsten (W) absorbers. The combination of Si and W choices makes possible the design and construction of a very compact calorimeter with highly granular and compact active layers. In the detectors at the ILC, the very-front-end (VFE) electronics of the calorimeters will be embedded in the detector units. The desired signal dynamic range in each channel goes from 0.5 MIP to 3000 MIPs, where the MIP acronym stands for the energy deposited by a minimum-ionizing-particle. To reduce overall power consumption, the SiW-ECAL will exploit the special bunch structure foreseen for the ILC with the e^+e^- bunches trains grouped in spills of ~ 1 -2 ms width separated by ~ 200 ms. The front-end electronics will only be enabled during the spills and the bias currents will be shut down between the spills. This technique is usually denominated power pulsing. The calorimeters are operated in self-trigger mode (each channel featuring an internal trigger decision chain) and zero suppression mode.

2 The SiW-ECAL technological prototype

The first SiW-ECAL prototype was the so called SiW-ECAL physics prototype. It was extensively tested between 2005 and 2011 at DESY, FNAL and CERN [9–14]. For the physics prototype, the VFE was placed outside the active area with no particular constraints in the power consumption. It consisted of 30 layers of Si as active material alternated with tungsten plates as absorber material. The active layers were made of a matrix of 3x3 Si wafers of 500 μm thickness. Each of these wafers was segmented in matrices of 6x6 squared channels of 10x10 mm^2 . The prototype was divided in 3 modules of 10 layers with different W depth per layer in each of these modules (0.4, 1.6 and 2.4 X_0) making a total of 24 X_0 . That very first prototype offered a signal over noise on the measured charge of 7.5 for MIP like particles.

The current prototype is called the SiW-ECAL technological prototype. It addresses the main technological challenges: compactness, power consumption reduction through power pulsing and VFE inside the detector. The study presented here extends considerably the work presented in Ref. [15] on an earlier version of the technological prototype that comprised e.g. four times less channels per layer. Further, in this earlier study the detector was still operated in continuous power mode. In this section we described in detail the main features and characteristics of the technological prototype.

2.1 Silicon sensors

The sensors consist of high resistivity (bigger than 5000 $\Omega\cdot\text{cm}$) silicon wafers with a thickness of $320 \pm 15 \mu\text{m}$. The size of the wafers is $9 \times 9 \text{ cm}^2$ and each of them is subdivided in an array of 256 PIN diodes of $5 \times 5 \text{ mm}^2$. A MIP traversing the PIN parallel to its normal will create $\sim 80 h^+e^-$ pairs per μm which corresponds to 4.1 fC. The original design of the silicon wafers included an edge termination made of floating guard-rings. It was observed in beam tests [16, 17] that the capacitive coupling between such floating guard-rings and the channels at the edge created not negligible rates of parasitic signals. events in tests with high energy beams (pions and electrons with energies

larger than 20-40 GeV) An R&D program together with Hamamatsu Photonics (HPK Japan) was conducted to study the guard-ring design as well as the internal crosstalk. It was concluded that using wafers without guard-ring and with a width of the peripheral areas lower than $500\mu\text{m}$ thanks to the use of stealth dicing technique, the amount of these squared events can be reduced to be at negligible level. For the setup described in this article we used different solutions for the edge terminations. For all of them, the expected rate of fake events is however negligible due to the low energy of the particle beam studied in the present article.

2.2 SKIROC: Silicon pin Kalorimeter Integrated ReadOut Chip

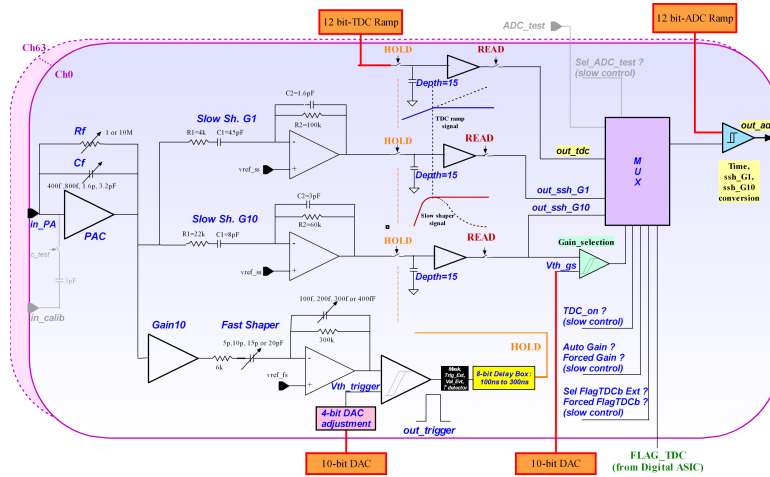


Figure 1. The schematics of the analog part of SKIROC2.

The SKIROC[18] (Silicon pin Kalorimeter Integrated ReadOut Chip) is a very front end ASIC (application-specific integrated circuits) designed for the readout of silicon PIN diodes. In its version SKIROC2 it consists of 64 channels in AMS $0.35\ \mu\text{m}$ SiGe technology. A schematic view of the analog part of the SKIROC2 is shown in Figure 1. Each channel comprises a low noise charge preamplifier of variable gain followed by two branches: a fast shaper for the trigger decision and a set of dual gain slow shapers for charge measurement. The gains can be controlled by modifying the feedback capacitance. When there is a trigger, the charge of the triggered channel is held after a fixed delay and stored in one of the memory cells of the 15 cell deep physical switched capacitor array (SCA). At the end of the slow clock period in which a trigger occurred the held of the charge of all the channels not triggered is launched. Finally, the signals are digitized by a Wilkinson type analogue to digital converter. The digitized information includes tags to identify the channels with and without trigger.

The SKIROC ASICs can be power-pulsed. Under conditions as designed for the ILC the power consumption is expected to be as low as 25mW . The power pulsing feature is used for all the results discussed in this paper.

2.3 Active Sensor Units

The entity of sensors, thin PCB (printed circuit boards) and ASICs is called Active Signal Units or ASU. An individual ASU has a lateral dimension of $18 \times 18\ \text{cm}^2$. The ASUs are currently equipped

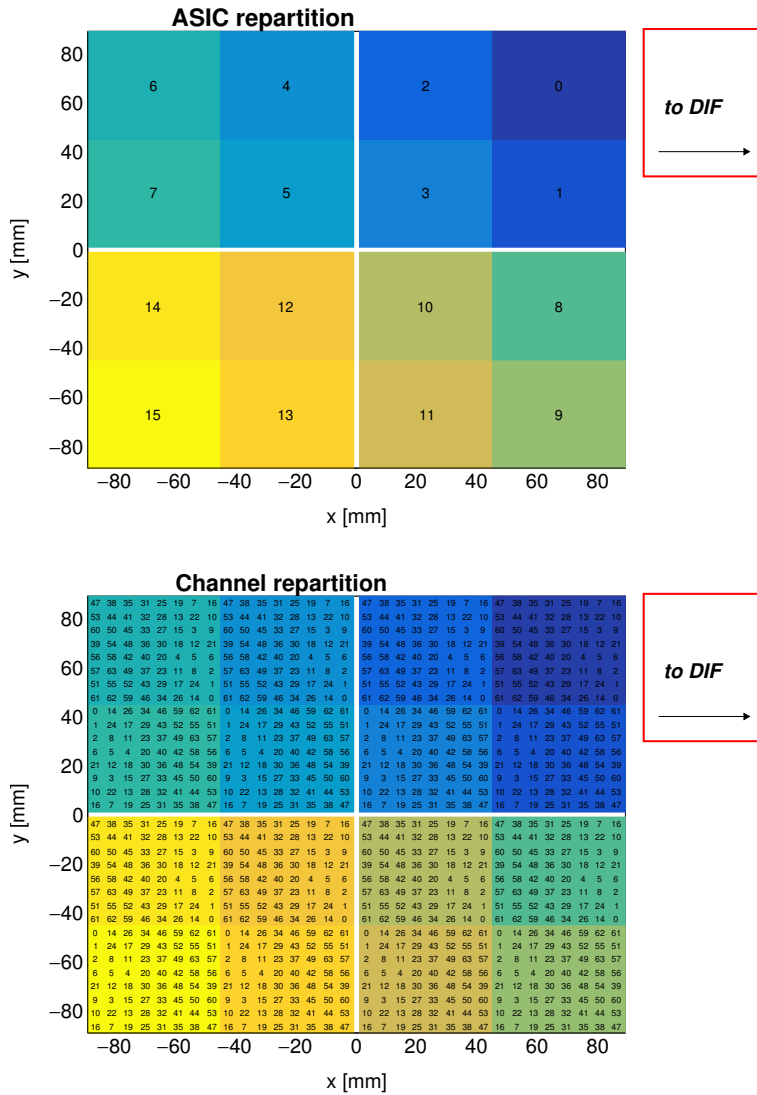


Figure 2. Repartition of the ASIC (up) and channels (down) in one ASU as viewed from the PCB side. The channels are separated (in x and y) by 5.5 mm^2 . The empty cross in the middle of the ASU corresponds to the 1 mm separation between the sensors. The areas covered by the different ASICs and channels are labeled with numbers following design and DAQ criteria: from 0-16 in the case of the ASICs and from 0-63 in the case of the channels.

further with 16 SKIROC2 ASICs for the read out and feature 1024 square pads (64 per ASIC) of $5.5 \times 5.5 \text{ mm}$. The channels and ASICs are distributed along the ASU as shown in Figure 2. Each ASU is equipped with 4 silicon wafers as the described in Section 2.1. The high voltage is delivered to the wafers using a HV-kapton sheet that covers the full extension of the wafers.

The current version of the PCB is called the FEV11. It has a thickness of 1.6 mm which grows up to 2.7 mm when the ASICs in its current packaging (1.1 mm thick LFBGA package) are bonded in top of it.

2.4 Data Acquisition system

The subsequent chain of the data acquisition (DAQ)[19] system consists of three components. They are enumerated from upstream to downstream from the data flow perspective:

1. The first component is the so called detector interface (DIF) which is placed at the beginning of each layer.
2. Each DIF is connected via a standard HDMI to the second component: a concentrator card called the Gigabit Concentrator Cards (GDCCs). These cards control up to 7 DIFs. They collect all data from the DIFs and distribute in turn the system clock and fast commands.
3. The most downstream component, is the clock and control card (CCC) which provides a clock, the control fan-out of up to 8 GDCCs and accepts and distributes external signals (i.e. signals generated external pulse generator to simulate the ILC spill conditions).

The whole system is controlled by the Calicoes and the Pyrame DAQ software version 3 [20, 21].

2.5 The prototype setup

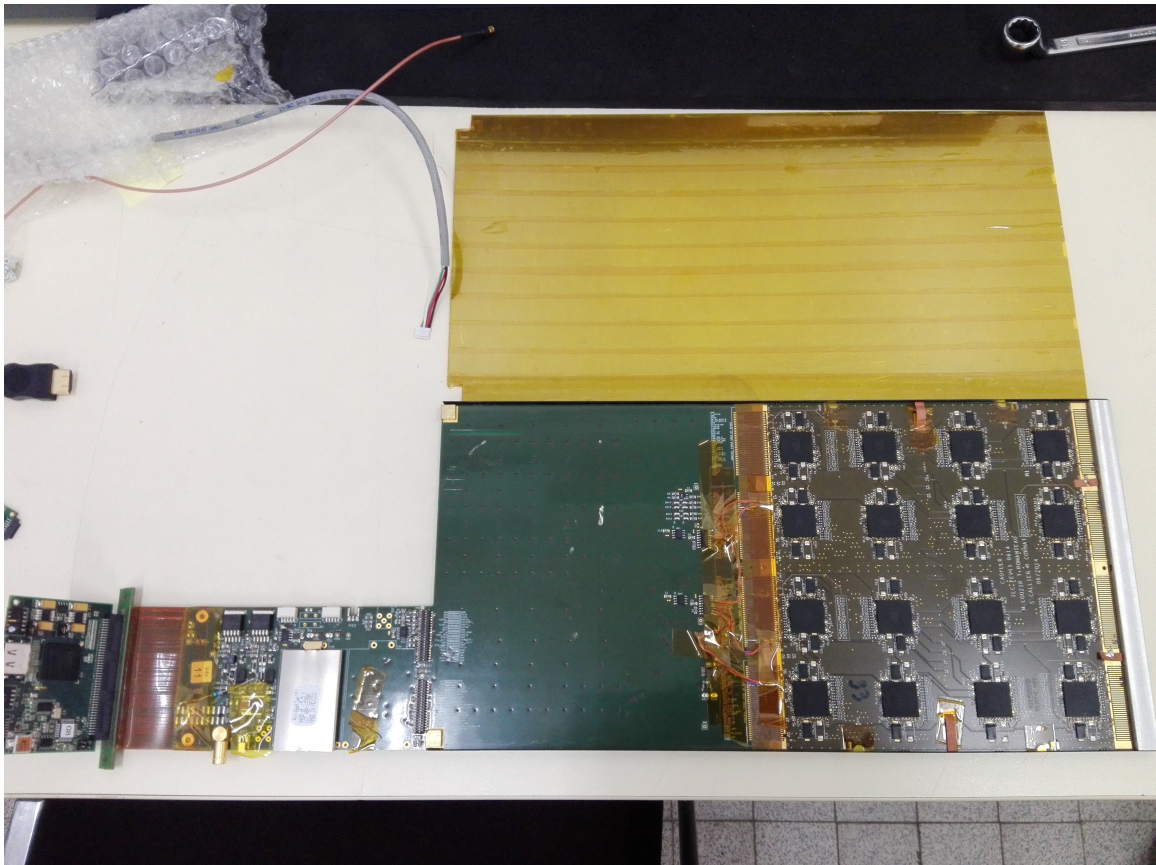


Figure 3. Open single readout layer with FEV11 ASU, 16 SKIROC 2 and the interface card visibles.

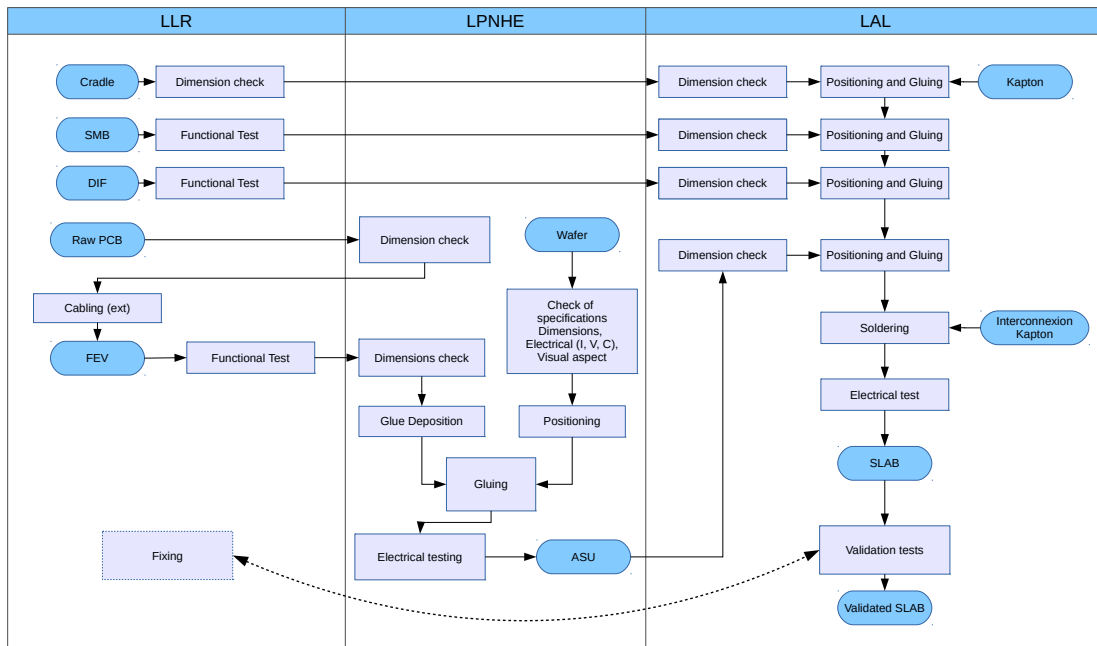


Figure 4. Process flow for the assembly of the SiW-ECAL readout layers.

A fully equipped readout module is shown in Fig. 3. These modules consist in this case of one ASU connected to a data acquisition system (DAQ) through an adapter board, called SMBv4. The ASU is the squared PCB on the right side, equipped with the 16 SKIROC2 bump bonded. It is connected with kapton connectors to the SMBv4 PCB which occupies the rest of the picture. The SMBv4 also holds other services e.g. the super capacitance used for the power pulsing. This decoupling capacitor (seen in the left bottom part of the photograph) of 400mF with 16 mΩ of equivalent serial resistance provides enough local storage of power to assure stable low voltage supply during the power pulsing. The readout modules are embedded on a "U" shaped carbon structure to protect the wafers. The full system is then covered by two aluminum plates to provide electromagnetic shielding and mechanical stability.

For the production of the small sample of readout modules studied in this document, a scalable working procedure has been established among several groups [22] profiting from the funding of projects like AIDA2020 or the HIGHTEC emblematic project of the P2IO. A schematic view of this assembly procedure chain can be seen in Figure 4. For more details we refer to Ref.[22].

A picture showing the SiW-ECAL technological prototype setup can be seen in Figure 5. The current prototype consists of 7 layers of readout layers housed in a PVC and aluminum structure that can host up to 10 layers in slots separated by 15 mm each. The first six layers were placed in the first six slots and the last one was in the last slot. In the following sections, we will refer to layers number 1 to 7, where the 1 is the most upstream of the beam. This setup is used for commissioning

(Section 3) and for the beam test (Section 4).

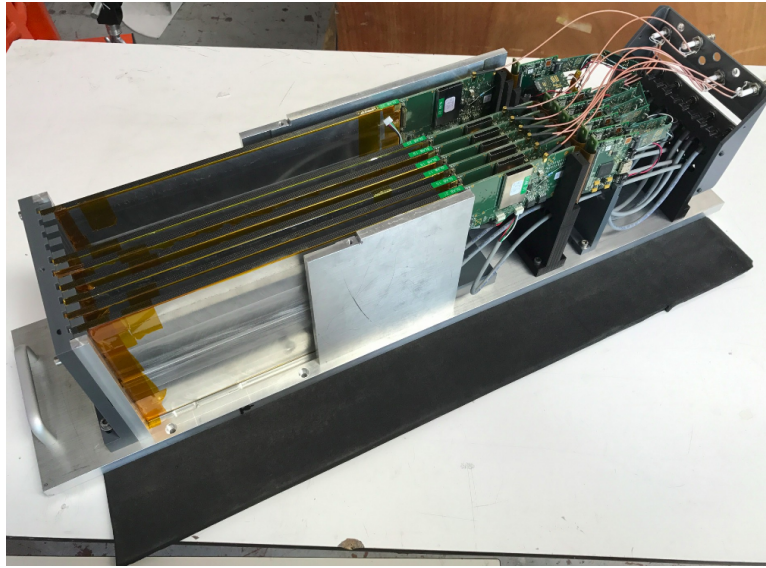


Figure 5. Prototype with 7 layers inside the aluminum stack.

3 Commissioning

Earlier experiences with the SKIROC2 ASIC are reported in Refs. [15, 23]). Internal SKIROC2 parameters reported in these references are adopted in the following unless stated otherwise. For example, a gain value of 1.2pF for the preamplifier is used. With this gain, the SKIROC2 features a linearity better than 90% for 0.5-200 MIPs, which is sufficient for electromagnetic showers created by few GeV electrons or positrons.

The main goal of the the commissioning procedure is the optimization of the trigger thresholds to levels in which we are able to record physics signals bellow the MIP level without saturating our DAQ with noise signals. This requires a careful and systematic procedure to:

1. identify the readout channels that are noisy in high trigger threshold above MIP signal conditions;
2. and select the optimal trigger threshold levels.

During the commissioning, we observed the repetition of coherent noise events affecting to several readout layers at the end of acquisitions with long gating time. The situation could be remedied by improving the isolation of the individual readout layers and by reducing the data taking to short gating times. In any case, all runs dedicated to the commissioning are usually characterized by their short gating windows for the acquisition (1-2ms) at low repetition frequencies (1-5 Hz) to minimize the chances of having real events due to cosmic rays during the data taking.

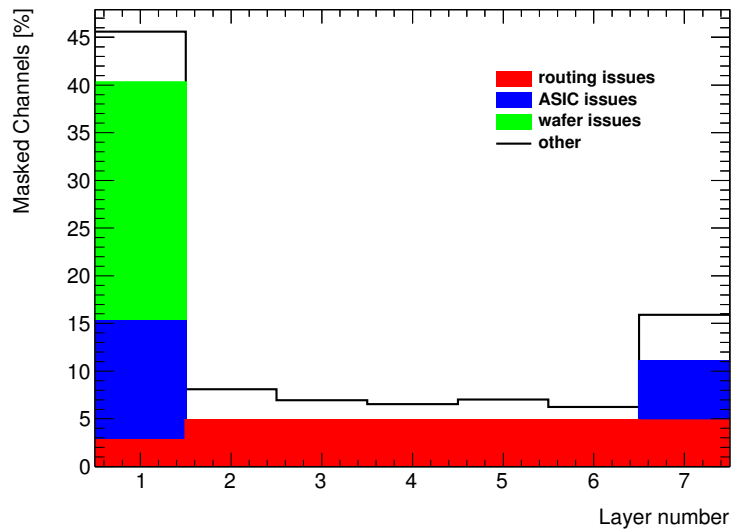


Figure 6. Fraction of channels that are tagged as noisy in all readout layers.

3.1 Tagging and control of the noisy channels.

The list of the noisy channels was obtained by means of dedicated data taking runs. In these runs we scan relatively high trigger thresholds from larger to lower values (*i.e.* between 1-3 MIPs) and progressively mask channels that exhibit counts. In each step, the decision of tagging a channel as noisy was taking following the rules described next:

- if the channel was triggered at rates larger than 0.5-1% of the total number of triggers per ASIC it was added to the list;
- if a channel was tagged as noisy in, at least, three of the readout layers, it was tagged as noisy for all and added to the list of channels being suspect of suffer from routing issues.

Following this procedure, we found two different types of noisy channels. One set consists of channels randomly distributed along the surface of every ASU and the other consists of channels located in specific areas and systematically noisy in all the ASUs. Preliminary inspections of the PCB layout hint that the channels in the latter set may be noisy due to improvable routing of the PCB. Deeper studies on the PCB routing must be conducted to clarify this. All the noisy channels have been identified and masked and the power of their preamplifiers has been disabled. All the results shown in the following sections are obtained in these conditions.

In addition to the different noisy channel types described above, we also have masked full sectors of the readout layers if an ASIC was tagged as faulty (at least 70% of channels listed as noisy) or if a Si-wafer was damaged (high leakage currents). The results of this study are summarized in Figure 6.

3.2 Optimal trigger threshold determination

After the noisy channels have been masked, dedicated trigger threshold scans are performed. The results are presented with the so-called the threshold scan curves where the x-axis represents the threshold value and the y-axis the number of recorded signals normalized to 1. The threshold values are given in internal DAC units which are translated to meaningful physical quantities in Section 3.3. In the absence of external signals (cosmic rays, injected signals, etc) the falling edge position in the threshold scan curves is due to the electronic noise at the output of the fast shaper (the trigger decision branch on the SKIROC) and it depends on the slow clock frequency. These threshold scan curves are approximated by a complementary error function:

$$\frac{2p_0}{\sqrt{\pi}} \int_{\frac{DAC-p_1}{p_2}}^{\infty} e^{-t^2} dt, \quad (3.1)$$

where p_0 is 1/2 of the normalization, p_1 is the value in which the noise levels are the 50% of its maximum and p_2 give us the width of the error function. In Figure 7 two threshold scans curves are shown together with the fit by the theoretical function.

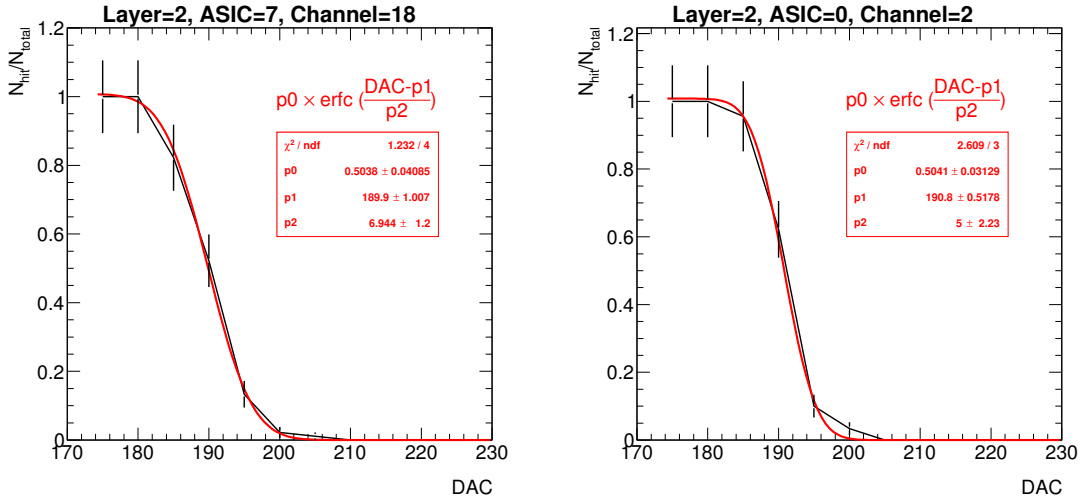


Figure 7. Two threshold scan curves.

For every ASICs, after performing the fit of the theoretical curves to the threshold scans, the average values of the p_1 and p_2 are calculated. These are represented by $\langle p_{1,2}^{ASIC} \rangle$ in the following. The optimal threshold value of every ASIC, in DAC units, was chosen using the following formula

$$DAC_{optimal}^{ASIC} = \text{maximum}(\langle p_1^{ASIC} \rangle + 5 \times \langle p_2^{ASIC} \rangle, 230). \quad (3.2)$$

This formula was applied if at least the the 30% of the 64 channels in the ASIC could be fitted. If not, a global threshold value of 250 was set.

The optimal trigger threshold values for all ASICs are shown in Figure 10, in internal DAC units and in MIPs. In the next section we explain how the conversion is done.

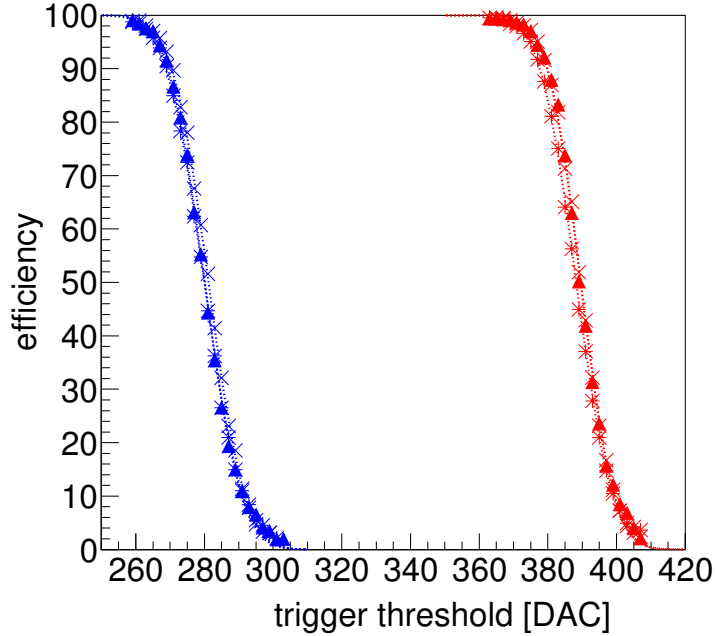


Figure 8. Threshold scan curves with charge injection (1 MIP in blue and 2 MIPs in red) for two different channels in a SKIROC2 testboard.

3.3 S/N ratio for the trigger decision

Performing threshold scans using real signals allows to calculate the signal over noise (S/N) ratio for the trigger decision. For that we compare the curves for 1 MIP and 2 MIP injected signals. The S/N is, in the following, defined as the ratio between the distance of both curves at its 50% and the width of the curves. The width is defined as the half of distance, in threshold units, between the curve at $50 \pm 34\%$. In Figure 8 we see the 1 MIP and 2 MIP curves obtained for several channel in a SKIROC testboard in which a single SKIROC2 in BGA package is placed and the 1 MIP and 2 MIPs size signals are directly injected in the preamplifier (via a 3 pF capacitor located in the injection line as shown in Figure 1).

We have obtained similar results using real signals, in this case cosmic rays signals. This is shown in Figure 9 where we show the result of the fit to the threshold scan curves cosmic rays integrated for all channels in one ASIC. For completeness, the fit of threshold scan curves for all channels in the same ASIC are also shown.

From these two results we extract the value of

$$S/N(trigger) = 12.9 \pm 3.4 \quad (3.3)$$

for the trigger decision. The central value is calculated from Figure 1 by the comparison of the 1 and 2 MIP curves and using the width of the 1 MIP curve in the denominator. The estimated uncertainty has two components: the difference of width between the 1 and 2 MIP curves of injected signals and the differences (width and middle point) between the 1 MIP curves for injected and cosmic ray signals. With this value of the S/N we are able to operate the internal trigger for small

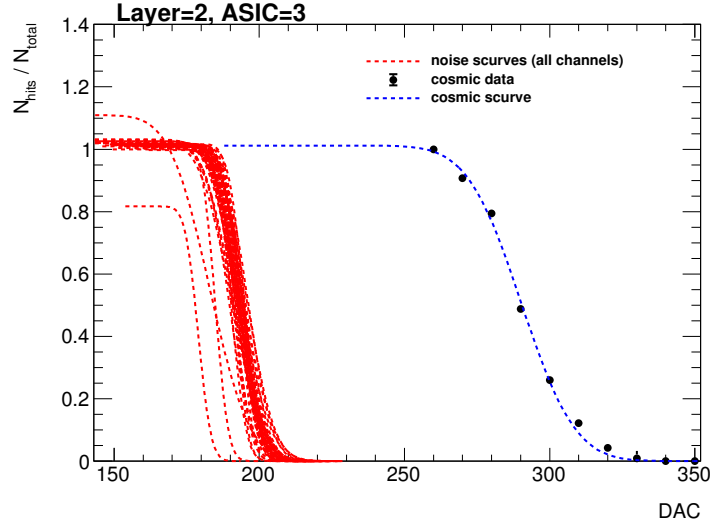


Figure 9. Threshold scan curves for noise (channel by channel, only the result of the fit) and cosmic rays (all channels together) for one ASIC in layer 2.

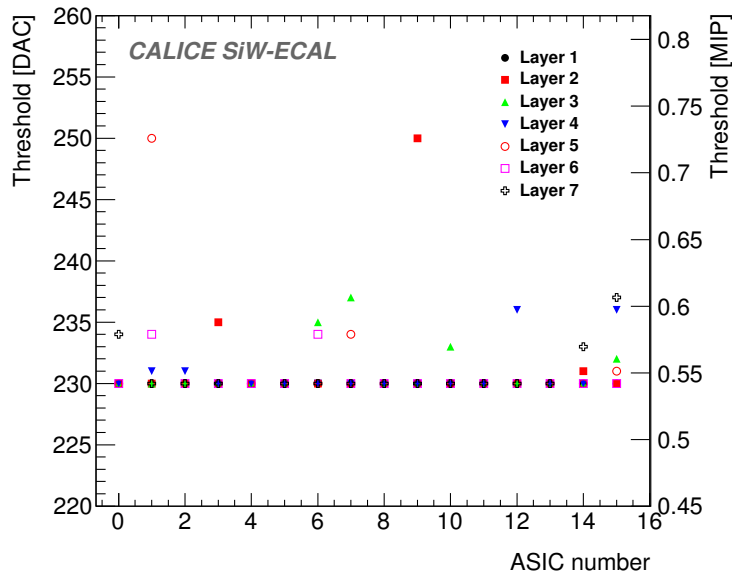


Figure 10. Summary of the trigger threshold settings in internal DAC units and in MIP units.

signals of the size of ~ 0.5 MIP. This is seen in 10 where the chosen thresholds of every ASIC being tested in beam are shown. However dedicated studies in beam test are needed in order to reduce the uncertainty of this measurement.

3.4 Prospects

The commissioning procedure described above relies on very conservative decisions due to the presence of unknown noise sources during largest of the commissioning phase. These sources

are now well known and therefore a new noise commissioning procedure has been studied. It will consist on an iterative algorithm that first will identify and mask the channels in which the number of triggers per channel will be compared with the number of expected triggers assuming only cosmic rays as signal. This will allow us to have a definition of the noise levels for each channel independently instead of relatively to the total number of triggers recorded by the ASIC. Finally, once the noisy channels are identified, the thresholds are further optimized with a last run for the identification of the residual noisy channels.

Using this new procedure we manage to reduce the number of masked channels by a factor of two without any loss of performance, at least in the laboratory and using 3 of the 7 readout layers. This new procedure will also be applied in the next beam test. Also, in order to optimize the commissioning of the detector, we propose a new set of measurements in the next beam test such as a threshold scan for the determination of the S/N in the trigger line. This can be done by the comparison of threshold curves taken with incident MIP-acting particles and MIP-acting particles traversing the detector tilted by 45 degrees with respect to the beam direction.

4 Performance in a beam test with positrons at DESY

The beam line at DESY provides continuous positron beams in the energy range of 1 to 6 GeV with rates from a few hundreds of Hz to a few kHz with a maximum of ~ 3 kHz for 2-3 GeV. In addition, DESY gives access to a bore 1 T solenoid, the PCMag.

The physics program of the beam test can be summarized in the following points:

1. Calibration without tungsten absorber using 3 GeV positrons acting MIPs directed to 81 position equally distributed over the modules.
2. Test in magnetic field up to 1 T using the PCMag. For this test a special PVC structure was designed and produced to support one single readout layer. The purpose of such test was twofold: first to prove that the DAQ, all electronic devices and the mechanical consistency of the readout layer itself are able to handle strong magnetic fields; second to check the quality of the data and the performance of the detector during the data taking when running in a magnetic field.
3. Response to electrons of different energies with fully equipped detector, i.e. sensitive parts *and* W absorber, with three different repartitions of the absorber material:
 - W-configuration 1: 0.6, 1.2, 1.8, 2.4, 3.6, 4.8 and 6.6 X_0
 - W-configuration 2: 1.2, 1.8, 2.4, 3.6, 4.8, 6.6 and 8.4 X_0
 - W-configuration 3: 1.8, 2.4, 3.6, 4.8, 6.6, 8.4 and 10.2 X_0

First reports on this beam test can be found in Refs. [24, 25]. These results have been extended and are discussed in the following sections. In Section 4.1 we discuss in detail the results of the pedestal, noise and MIP calibration. We show also results on the pedestal and noise stability when running inside a magnetic field in Section 4.2 and in electromagnetic shower events in Section 4.3. The study of the calibration of the prototype in electromagnetic shower events is due to a future publication.

4.1 Noise study and MIP calibration

In Figure 11 we show the signal and pedestal distribution of a single channel after subtracting the pedestal mean position. The results of the MIP calibration fit are shown in red. The signal distribution is integrated over all SCAs. For cosmetic reasons the pedestal distribution is shown only for the first SCA.

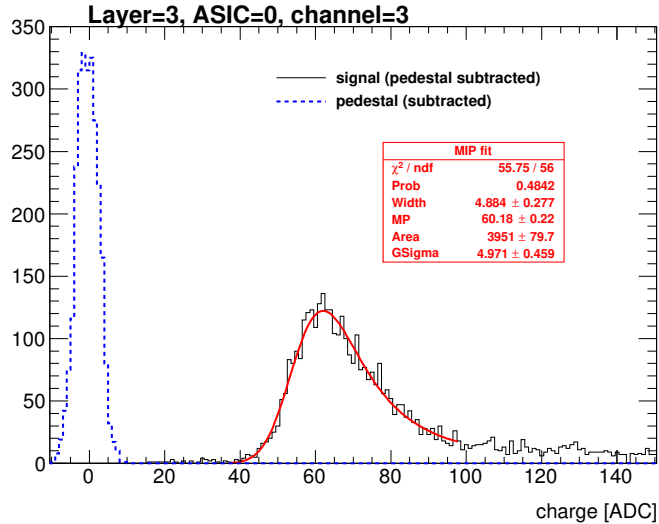


Figure 11. Pedestal (blue dashed line) and signal (black continuous line) distribution for one channel in the third layer.

The pedestal is calculated as the mean position of the distribution of the ADC values for all channels without trigger. The noise is associated to the width of the distribution. The pedestal correction is done layer-, chip-, channel- and SCA-wise due to the large spread of values between pedestals, as observed in Figure 12 (left plot) and Figure 13 (also left plot). For the noise, the dispersion is much smaller ($\sim 5\%$). This is shown in the right plots of Figures 12 and 13. From now on, the pedestal correction is applied to all the results presented. The resulting spectra are fit by a Landau function convoluted with a Gaussian. The most-probable-value of the convoluted function is taken as the MIP value, allowing thus for a direct conversion from ADC units to energy in MIP units. The fit succeeded in 98% of the cases and the spread of the resulting MPV is 5%. The remaining channels will be discarded. Results are summarized in figure 14, leftmost plot.

The Figure 15 shows the response of all channels integrated over the calibration run. This plot is obtained after further refinement of the sample by selecting incident tracks. The maximum peaks at 1 MIP as expected after a good calibration. In addition to this, a second and a third peaks are visible as shoulders. These shoulders are associated to events involving multiple particles crossing the detector.

To evaluate the single hit detection efficiency we define a high purity sample of events by selecting tracks with at least 4 layers with a hit in exactly the same channel. Afterwards we check which layers have or not a hit in the same or in the closest neighboring channels with energy larger or equal than 0.3 MIP. We repeat this procedure for all channels. The results are shown in Figure

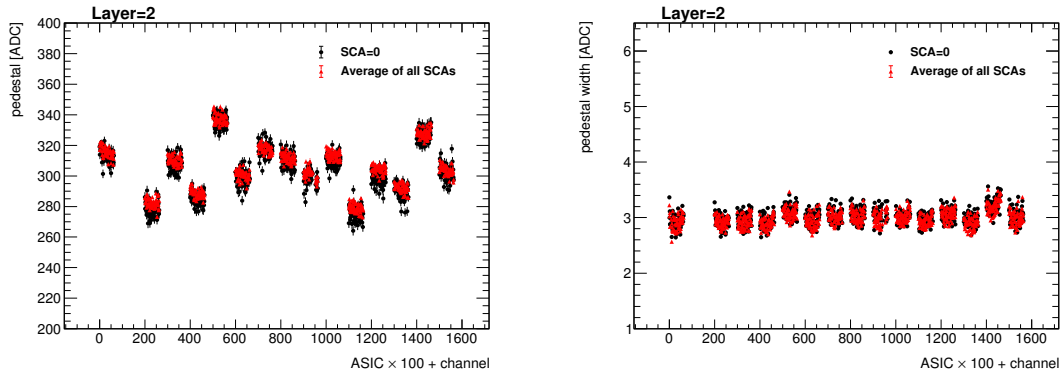


Figure 12. Upper plots: pedestal mean position (left plot) and width (right plot) for all channels in one layer. Lower plots: same plots but after subtracting the corresponding averaged values calculated for each ASIC and SCA.

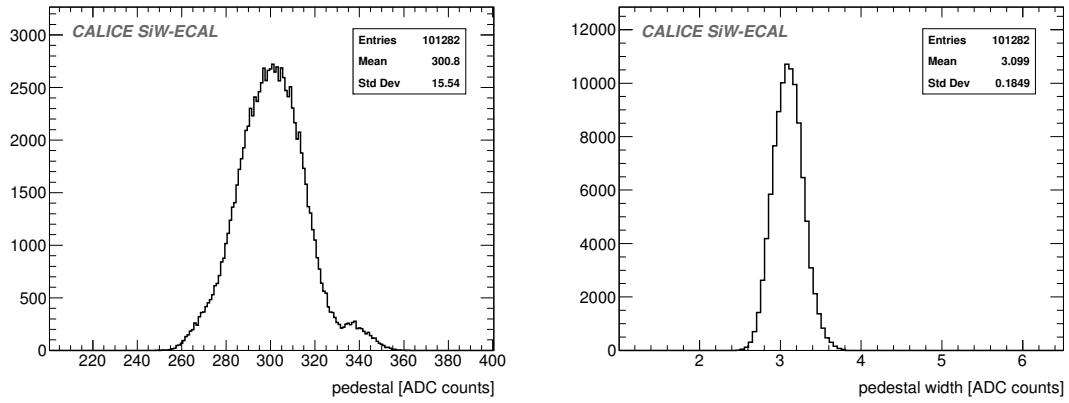


Figure 13. Pedestal mean position (left) and width (right) for all channels and all SCAs in the setup.

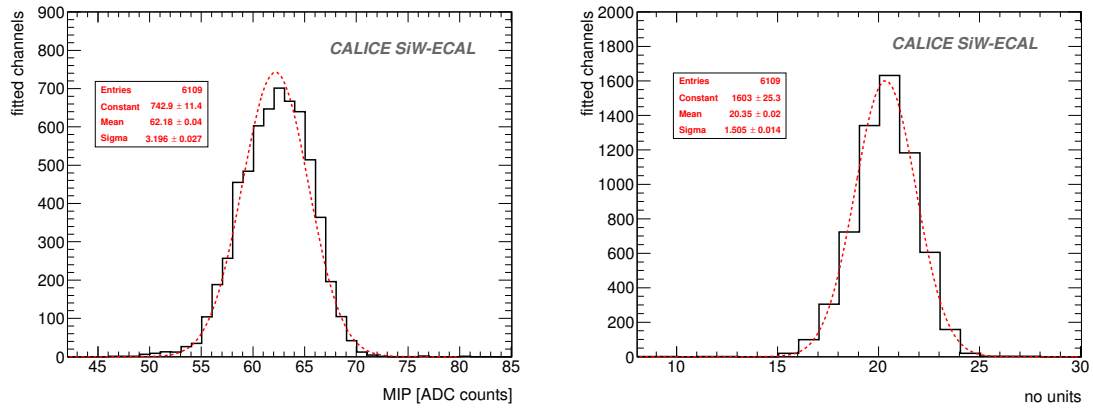


Figure 14. Result of the MIP position calculation and signal over noise for the charge measurement on triggered channels for all calibrated channels.

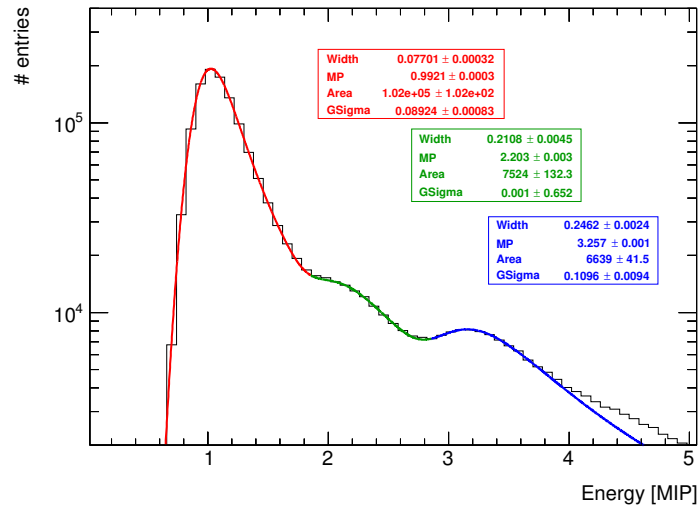


Figure 15. Energy distribution for all calibrated channels when selecting incident tracks of 3 GeV positron acting as MIPs.

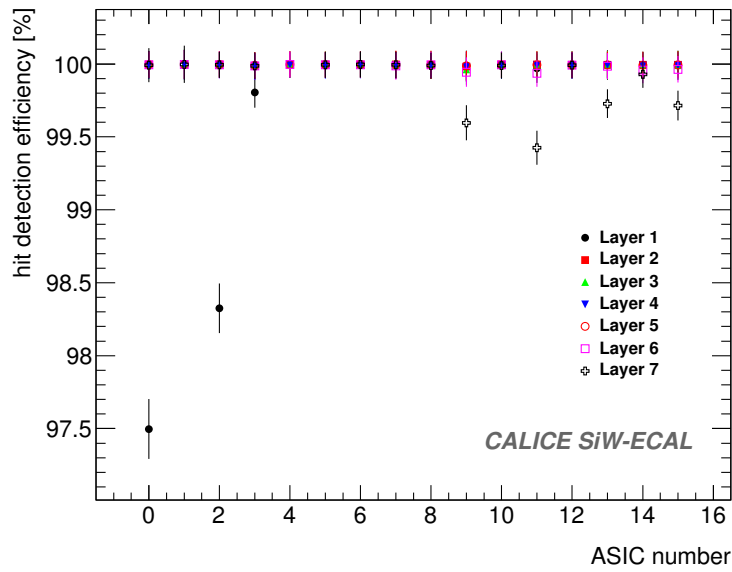


Figure 16. MIP detection efficiency for all layers and ASICs in high purity samples of tracks of MIP-like acting particles.

16. Except few exceptions, the efficiency is compatible with 100%. The low efficiencies in the first layer are related to the presence of noisy channels not spotted during the commissioning. These channels may saturate de acquisition in their ASICs. In the last layer we also observe a few small deviations which are associated to the outliers channels, hinting for a small misalignment of the last layer.

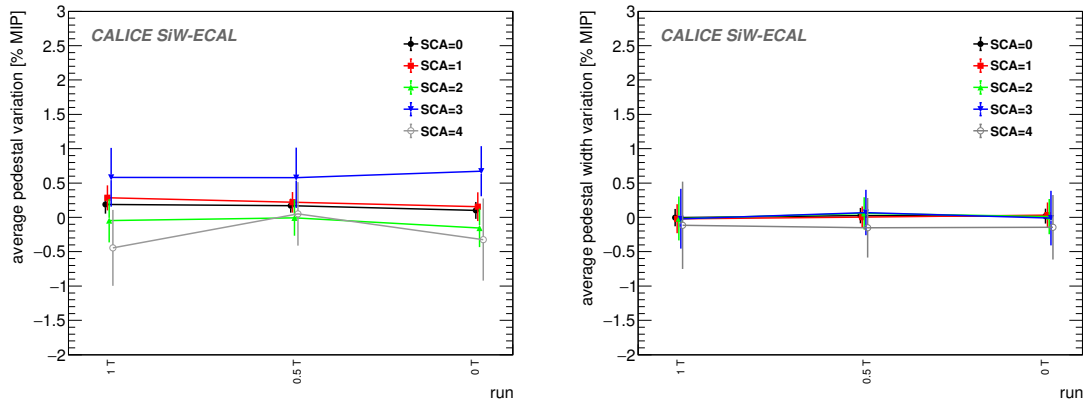


Figure 17. Average deviation of the pedestal mean position (left) and width (right) for all channels in the ASIC 12.

4.1.1 S/N for the charge measurement of triggered channels

The S/N for the charge measurement of triggered channels is defined as the ratio between the most-probable-value of the Landau-gauss function fit to the data (pedestal subtracted) and the noise (the pedestal width). This quantity has been calculated for all channels and all layers. Results are summarized in Figure 14, rightmost plot. The large size of this value allows us to filter out small spurious triggers with high efficiency.

4.2 Pedestal and noise stability in a magnetic field

The data taking inside the magnetic field has been divided in three runs:

1. a with a magnetic field of 1 T;
2. a run with 0.5 T;
3. and a final run with the magnet off.

The beam, 3 GeV positrons, was directed in the area of the PCB readout by the ASIC number 12. The pedestal positions and noise levels of the channels of the ASIC 12 when the readout layer is inside of the PCMag are compared with the results from the calibration run described in the previous section. This is shown in Figure 17. We see that the agreement is perfectly good within the statistical uncertainties. Due to the lower rates in this beam area, the analysis is only done up to few SCAs.

4.3 Pedestal stability in electromagnetic shower events

In this section we discuss the pedestal stability in events with large amount of charge collected by the ASICs, as are the electromagnetic shower events. All the results shown in this section correspond to data taken during the tungsten program, using the W-configuration number 2 when shooting the beam in the area registered by the ASIC 12 (and partially in the 13). For simplicity, only information recorded by ASIC 12 will be shown. In order to select a high purity of electromagnetic shower like

the events, we used a simple criteria: select only events with at least 6 of the layers with at least a hit with $E > 0.5$ MIP.

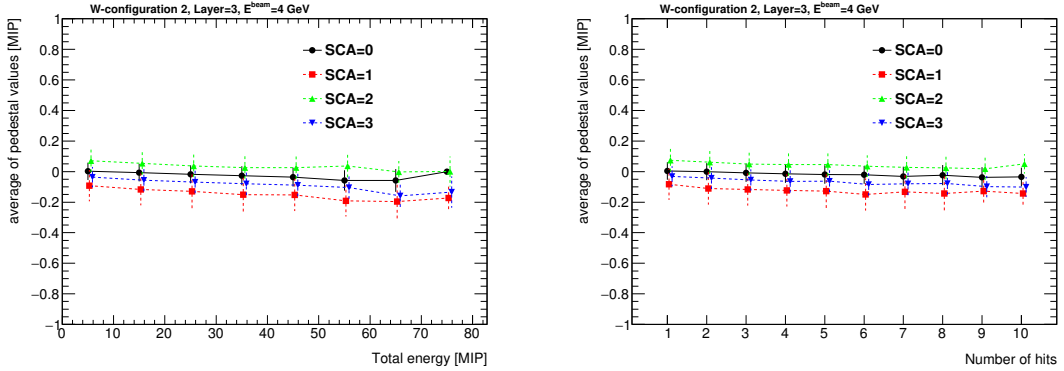


Figure 18. Left: mean position of the projection of the pedestal distribution of all channels calculated when different energies are collected in the ASIC (in bins of 10 MIPs). Right: same but as a function of the number of hits. In both cases, the results are shown for few SCA. The points for the curves with SCA different than zero are slightly shifted in the x-axis to optimize the visualization.

Two main observations have been extracted from the recalculation of the pedestals and its comparison with the values obtained previously during the calibration runs. The first observation consists in a relatively small drift of the pedestal values towards lower values when the collected energy is high *i.e.* when the number of triggered channels is large. This is shown in Figure 18 for several SCAs. A small dependence, in all SCAs, of the pedestal position on the amount of charge collected by the ASIC is observed. This feature is known and it is due to the architecture of the SKIROC2 ASICs where high inrush of currents can slightly shift the baseline of the analogue power supply. The second observation extracted from this analysis can be also seen in Figure 18 but more clearly in Figure 19: in addition to the small drift of the pedestal value an SCA-alternate global shift is observed. We see that the effect is enhanced when large amounts of charge are deposited in the ASIC (*i.e.* at larger beam energies or for the layers in the maximum of the shower profile). We also observed that this alternation is only SCA dependent and does not depends on the time in which the deposit of energy occurs within the acquisition. This is not yet fully understood although the fact that the effect is observed in alternate SCAs hints that something is affecting to the digital part of the ASIC (where the SCAs enter in play). Dedicated tests in the laboratory and in the beam are needed in order to clarify this issue.

5 Summary

The R&D program of the highly granular SiW-ECAL detector is in an exciting phase. After the proof of principle of the imaging calorimetry concept using the physics prototype, the technological prototype is being constructed and tested. In this document we describe the commissioning and beam test performance of a prototype built in with the first fully assembled detector elements, in contrast with previous beam tests. In addition, with the setup used in this beam test we reached levels of granularity similar to the targets of the ILD detector for the ILC. This is also the first

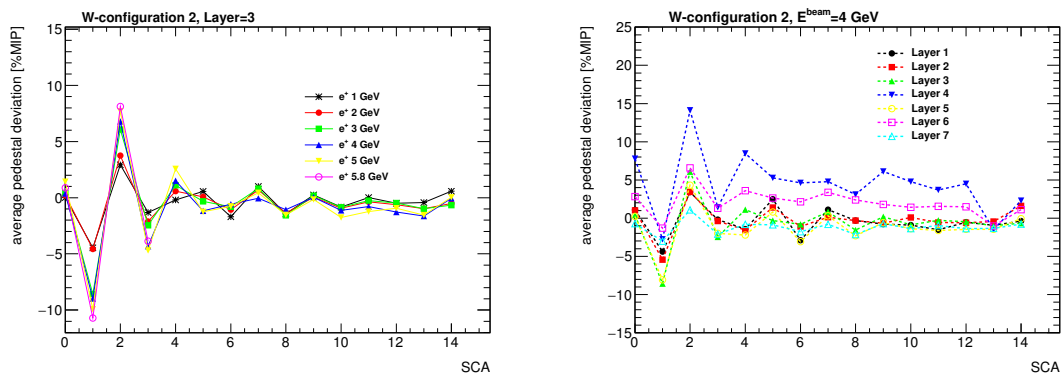


Figure 19. Average value over all channels in ASIC 12 of the pedestals position for each SCA in electromagnetic shower events.

time that results with the SiW-ECAL prototype continuously working in power pulsing mode are published. Finally, we tested the performance of the detector modules working for long periods inside magnetic fields.

The beam test has provided a lot of useful data to study the performance of the detector and to perform a channel by channel calibration, showing a good homogeneity with a spread of the 5% for all channels. The S/N on the trigger has been evaluated to be 12.9 ± 3.4 . The S/N on the charge measurement of triggered cells is 20.4 ± 1.5 . The hit detection efficiency in tracks has been evaluated to be compatible with 100%.

6 Outlook

In parallel to the work described here, several R&D efforts are being carried. One of these efforts is directed to the design and test of new ASICs. In fact, a new generation of the SKIROC, the 2a, has been delivered, tested in the dedicated testboards and it has been integrated in new ASUs. In addition, a new generation of the ASIC, SKIROC3, is foreseen for the final detector construction. In contrast with SKIROC2/2a, the new ASIC will be fully optimized for ILC operation, *i.e.* full zero suppression, reduced power consumption etc.

Many efforts are also concentrated in the construction and test of long readout layers made of several ASUs enchainned since we know that the ILD ECAL will host long layers of up to ~ 2.5 m. This device constitutes a technological challenge in both aspects, the mechanical (very thin and long structure with fragile sensors in the bottom make complicated the assembly procedure and the handling...) and the electrical (we need to ensure and control the transmission of signals and high currents along the full device). For example, interconnections between ASUs and between ASU and interface card are one of the most involved parts of the assembly and require close collaboration between mechanical and electronic engineers. A first long readout layer prototype of ~ 8 ASUs has been already tested in beam test also in DESY in 2018.

In parallel, a different proposal for a thinner ASU design is being investigated. This is motivated by the high density of channels demanded by the Particle Flow algorithms. In this alternative PCB design the ASICs are directly placed on board of the PCB in dedicated cavities. The ASICS will be

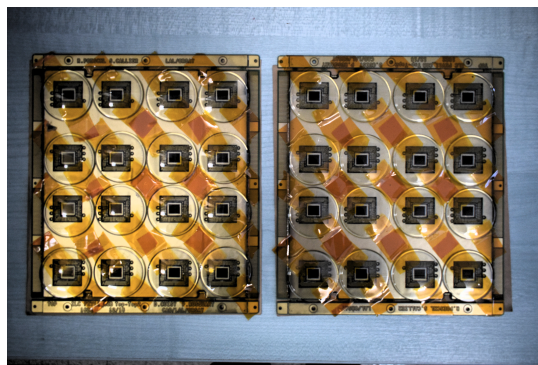


Figure 20. Two FEV11_COB boards with 16 SKIROC2a wire bonded. The ASICs are protected with watch glasses.

in semiconductor packaging and wire bonded to the PCB. This is the so-called COB (chip-on-board) version of the ASU. A small sample of FEV11_COBs (same connexion pattern with the interface card than FEV11) with a total thickness of 1.2 mm (to be compared with the 2.7 mm of the LFBGA solution in the FEV11) has been produced and tested in the laboratory showing its readiness for tests with particle beams. A sample can be seen in Figure 20.

Finally, intensive R&D on the compactification of the DAQ to meet the tight space requirements for the ILD is being done by the SiW-ECAL collaboration.

It is foreseen that all these developments, with the exception of the SKIROC3, will be tested with particle beams during 2018-2019.

Acknowledgments

This project has received funding from the European Union's Horizon 2020 Research and Innovation program under Grant Agreement no. 654168. This work was supported by the P2IO LabEx (ANR-10-LABX-0038), excellence project HIGHTEC, in the framework 'Investissements d'Avenir' (ANR-11-IDEX-0003-01) managed by the French National Research Agency (ANR). The research leading to these results has received funding from the People Programme (Marie Curie Actions) of the European Union's Seventh Framework Programme (FP7/2007-2013) under REA grant agreement, PCOFUND-GA-2013-609102, through the PRESTIGE programme coordinated by Campus France. The measurements leading to these results have been performed at the Test Beam Facility at DESY Hamburg (Germany), a member of the Helmholtz Association (HGF).

A Appendix: Filtering of fake triggers

Several types of fake signals have been observed in the technological prototype since its construction and test. A detailed description of them can be found in previous articles, as for example, in Ref. [15]. All these fake signals are easily identified and tagged during the data acquisition and removed afterwards from the analysis not introducing any significance loss of performance as can be seen, for example, in the hit detection efficiency plots (see Section 4.1). In the following, we briefly describe the status of the monitoring, debugging and filtering of such kind of events.

Empty triggers

Empty trigger events are a well known feature of SKIROC2. The SKIROC2 uses an OR64 signal to mark the change to a new SCA when a signal over threshold is detected. The empty triggers appear when during the acquisition the rising edge of the slow clock falls during the OR64 signal and therefore the change to a new SCA is validated twice. This effect creates around 17% of empty events which are easily filter and removed from the analysis. The ratio of empty triggers in the new SKIROC2a has been reduced to the $\sim 2 - 3\%$ by reducing the length of the OR64 signal.

Plane events and retriggers

Another well know issue is the appearance of bunches of consecutive fake triggers, called retriggers, that saturates the DAQ. Although the ultimate reason of the appearance of these events remains not clear, it is suspected that they are related to distortions of the power supply baselines. We know that the SKIROC2 and 2a preamplifiers are referenced to the analog power supply level, therefore, any voltage dip can be seen as signal by the preamplifiers. Moreover the presence of a high inrush of current due to many channels triggered at the same time can create these voltage dips and also produce the so called plane events (most of the channels triggered at once). In previous studies the ratio of retriggers and plane events was reduced by improving the power supply stabilization capacitances.

Studying the MIP calibration data of this beam test we have noticed that the concentration of the retriggers and plane events in ASICs far from the beam spot is higher than in the ASICs that are reading out the information of real hits. We have also observed that the concentration of these events is higher in the nearby of channels that were masked as suspicious of suffering from routing issues. The ratio these events have been estimated to be of $1 - 3\%$ in the ASICs where high frequency interactions are produced (*i.e.* using 3 GeV positrons at 2-3 kHz) and at higher rates even larger than 40% in other ASICs far from the beam spot. Moreover, it has been noticed a correlation between the time that an ASIC was full and the time of the appearance of some retriggers in other areas of the PCB. This correlation corresponds to $\sim 1.6 \mu\text{s}$ which hints of a distortion on the analogue power supply when the signal that informs the DIF that one ASIC memory is full is transmitted through the PCB.

References

- [1] T. Behnke, J. E. Brau, B. Foster, J. Fuster, M. Harrison, J. M. Paterson et al., *The International Linear Collider Technical Design Report - Volume 1: Executive Summary*, [1306.6327](#).
- [2] H. Baer, T. Barklow, K. Fujii, Y. Gao, A. Hoang, S. Kanemura et al., *The International Linear Collider Technical Design Report - Volume 2: Physics*, [1306.6352](#).
- [3] C. Adolphsen, M. Barone, B. Barish, K. Buesser, P. Burrows, J. Carwardine et al., *The International Linear Collider Technical Design Report - Volume 3.I: Accelerator & in the Technical Design Phase*, [1306.6353](#).
- [4] C. Adolphsen, M. Barone, B. Barish, K. Buesser, P. Burrows, J. Carwardine et al., *The International Linear Collider Technical Design Report - Volume 3.II: Accelerator Baseline Design*, [1306.6328](#).
- [5] H. Abramowicz et al., *The International Linear Collider Technical Design Report - Volume 4: Detectors*, [1306.6329](#).

- [6] J.-C. Brient and H. Videau, *The Calorimetry at the future $e^+ e^-$ linear collider*, *eConf* **C010630** (2001) E3047, [[hep-ex/0202004](#)].
- [7] V. Morgunov and A. Raspereza, *Novel 3-D clustering algorithm and two particle separation with tile HCAL*, in *Linear colliders. Proceedings, International Conference, LCWS 2004, Paris, France, April 19-23, 2004*, pp. 431–436, 2004. [physics/0412108](#).
- [8] F. Sefkow, A. White, K. Kawagoe, R. Pöschl and J. Repond, *Experimental Tests of Particle Flow Calorimetry*, *Rev. Mod. Phys.* **88** (2016) 015003, [[1507.05893](#)].
- [9] CALICE collaboration, C. Adloff, J. Blaha, J. J. Blaising, C. Drancourt, A. Espargiliere, R. Galione et al., *Tests of a particle flow algorithm with CALICE test beam data*, *JINST* **6** (2011) P07005, [[1105.3417](#)].
- [10] CALICE collaboration, J. Repond et al., *Design and Electronics Commissioning of the Physics Prototype of a Si-W Electromagnetic Calorimeter for the International Linear Collider*, *JINST* **3** (2008) P08001, [[0805.4833](#)].
- [11] CALICE collaboration, C. Adloff et al., *Response of the CALICE Si-W electromagnetic calorimeter physics prototype to electrons*, *Nucl. Instrum. Meth.* **A608** (2009) 372–383, [[0811.2354](#)].
- [12] C. Adloff et al., *Study of the interactions of pions in the CALICE silicon-tungsten calorimeter prototype*, *JINST* **5** (2010) P05007, [[1004.4996](#)].
- [13] CALICE collaboration, C. Adloff et al., *Effects of high-energy particle showers on the embedded front-end electronics of an electromagnetic calorimeter for a future lepton collider*, *Nucl. Instrum. Meth.* **A654** (2011) 97–109, [[1102.3454](#)].
- [14] CALICE collaboration, B. Bilki et al., *Testing hadronic interaction models using a highly granular silicon–tungsten calorimeter*, *Nucl. Instrum. Meth.* **A794** (2015) 240–254, [[1411.7215](#)].
- [15] M. S. Amjad et al., *Beam test performance of the SKIROC2 ASIC*, *Nucl. Instrum. Meth.* **A778** (2015) 78–84.
- [16] CALICE collaboration, R. Cornat and R. Pöschl, *Technological prototype of a silicon-tungsten imaging electromagnetic calorimeter*, *JINST* **10** (2015) C06015.
- [17] CALICE collaboration, R. Cornat, *Semiconductor sensors for the CALICE SiW EMC and study of the cross-talk between guard rings and pixels in the CALICE SiW prototype*, *J. Phys. Conf. Ser.* **160** (2009) 012067.
- [18] S. Callier, F. Dulucq, C. de La Taille, G. Martin-Chassard and N. Seguin-Moreau, *SKIROC2, front end chip designed to readout the Electromagnetic CALorimeter at the ILC*, *JINST* **6** (2011) C12040.
- [19] F. Gastaldi, R. Cornat, F. Magniette and V. Boudry, *A scalable gigabit data acquisition system for calorimeters for linear collider*, *PoS TIPP2014* (2014) 193.
- [20] M. Rubio-Roy, F. Thiant and F. Magniette, *Flexible online monitoring for high-energy physics with Pyrame*, *J. Phys. Conf. Ser.* **898** (2017) 032009.
- [21] CALICE collaboration, F. Magniette and A. Irls, *Pyrame 3, an online framework for Calice SiW-Ecal*, *JINST* **13** (2018) C03009.
- [22] V. Boudry, R. Cornat, D. Lacour, R. Pöschl and F. Magniette, *Advanced assembly chain for Si calorimeters*, .
- [23] T. Suehara et al., *Performance study of SKIROC2/A ASIC for ILD Si-W ECAL*, *JINST* **13** (2018) C03015, [[1801.02024](#)].

- [24] CALICE collaboration, A. Irles, *Latest R&D news and beam test performance of the highly granular SiW-ECAL technological prototype for the ILC*, *JINST* **13** (2018) C02038, [[1802.08806](#)].
- [25] CALICE collaboration, A. Irles, *Latest developments on the highly granular Silicon-Tungsten Electromagnetic Calorimeter technological prototype for the International Large Detector*, in *2017 IEEE Nuclear Science Symposium and Medical Imaging Conference (NSS/MIC 2017) Atlanta, Georgia, USA, October 21-28, 2017*, 2018. [1801.10407](#).